Science & Technology Development Journal 2025, 28(4):3903-3910

Open Access Full Text Article

Research Article

The effect of chitosan molecular weight and concentration on the fabrication and performance of dissolving microneedles

Bao Nhien Au[1,2], Thuy Linh Thi Ta[1,2], Thanh Qua Nguyen[1,2], Long Binh Vong[1,2,*]

ABSTRACT

Dissolving microneedles (MNs) have received a significant amount of interest due to their ability to encapsulate and release drug formulations upon dissolution. This study investigated how the molecular weight of chitosan, a key component of dissolving MNs due to its high biodegradability and biocompatibility, influences the fabrication and transdermal performance of chitosan-based MNs. Chitosan MNs were fabricated using the double-casting method with chitosan solutions of different concentrations (0.5%, 1.5%, and 3% w/v) and molecular weights (low, medium, and high). PVA/PVP solution was used as the supporting base. Several key characteristics of the fabricated chitosan MNs were assessed, revealing that the morphology, mechanical strength, and skin insertion characteristics of chitosan MNs were greatly influenced by their molecular weight and concentration. All MNs exhibited well-formed microneedle structures, but only the 3% (w/v) chitosan formulations possessed the mechanical strength required for skin penetration. Among them, low molecular weight chitosan at 3% w/v concentration (3LW) exhibited the highest mechanical strength (95.97 mN) and greatest insertion depth (0.52 mm), with over 40% penetration into the fourth parafilm layer. Rhodamine B-loaded 3LW MNs exhibited an initial burst release (61% in 10 minutes) followed by sustained release (81% over 24 hours). Cytotoxicity testing confirmed the low toxicity of chitosan MNs against L929 fibroblasts. These findings suggest that 3LW chitosan MNs represent a promising platform for safe and effective transdermal drug delivery.

Key words: microneedles, chitosan, molecular weight, transdermal drug delivery

[1]*School of Biomedical Engineering, International University, Ho Chi Minh City 700000, Vietnam*

[2]*Vietnam National University Ho Chi Minh City, Ho Chi Minh City 700000, Vietnam*

Correspondence

Long Binh Vong, School of Biomedical Engineering, International University, Ho Chi Minh City 700000, Vietnam

Vietnam National University Ho Chi Minh City, Ho Chi Minh City 700000, Vietnam

Email: vblong@hcmiu.edu.vn

History

- Received: 28-03-2025
- Revised: 14-08-2025
- Accepted: 19-09-2025
- Published Online: 19-12-2025

DOI :

https://doi.org/10.32508/stdjet.v28i4.4444

INTRODUCTION

The skin is a potential site for drug absorption due to its large surface area. Drugs can be released into the skin through the application of drug-containing dosage forms[1]. Traditional topical and transdermal systems include creams, lotions, ointments, liniments, patches, and hypodermic needles[2]. These formulations have been widely used for the treatment of skin problems but present several limitations. In particular, these formulations have varying drug-carrying capacities, efficiencies, bioavailability, and patient compliance issues. For example, topical cream mainly spreads on the skin surface: only 10–20% of the total drug loaded in topical cream is absorbed through the skin[3]. Drugs in transdermal patches must cross the stratum corneum barrier, reducing its bioavailability; the addition of a permeation enhancer can improve delivery, but only slightly[4]. Conventional hypodermic needles are also widely used for transdermal drug delivery; however, needles require trained personnel for administration, and the pain associated with needles significantly reduces patient acceptance of this drug delivery method[5].

Microneedles (MNs) represent a novel technique that can overcome many of the limitations of conventional approaches to transdermal drug delivery and have recently become the subject of numerous studies. MNs are micron-sized projections that are typically assembled on a supporting base or patch. A typical microneedle has a tapered, sharp tip measuring 150–1500 μm in length, 50–250 μm in width, and 1–25 μm in thickness. Their tips may be triangular, rounded, or arrow-shaped[6]. There are four types of MN in the literature: solid[7], coated[8], hollow[9], and dissolving MNs[10].

In particular, dissolving MNs have attracted a significant amount of interest in recent years. The key feature of dissolving MNs is that the drug formulation is encapsulated within their structure and released as the MNs dissolve[11]. Dissolving MNs are generally composed of soluble materials or biodegradable polymers, allowing them to be used for controlled drug delivery, i.e., drug delivery rates can be tailored according to patient requirements[12]. They can also be designed with specific arrays that allow for rapid dissolution, making them a viable option for applications such as drug delivery to the eye or vaccination [13]. Alternatively, slower dissolution processes can be used in

Cite this article : Au B N, Ta T L T, Nguyen T Q, Vong L B. **The effect of chitosan molecular weight and concentration on the fabrication and performance of dissolving microneedles**. *Sci. Tech. Dev. J.* 2025; 28(4):3903-3910.

cases requiring slower drug delivery over an extended time [13].

Chitosan was selected as the matrix material in dissolving MN fabrication due to its suitability for transdermal drug delivery. Like other biopolymers, chitosan is biocompatible, biodegradable, and low in toxicity, while offering several unique advantages [14]. Firstly, its cationic nature facilitates mucoadhesion and enhances transient interactions with negatively charged cell membranes, allowing it to reversibly open tight junctions and improve the paracellular transport of encapsulated drugs [15]. Chitosan also exhibits intrinsic antimicrobial activity, which can reduce the risk of infection at the application site [16].

Previous studies reported that the molecular weight of chitosan affected its structure, stability, and water solubility [17]; however, few studies have been conducted to determine the specific effect that the molecular weight of chitosan has on transdermal delivery in dissolving chitosan MNs. This study aims to investigate how the molecular weight and concentration of chitosan affect the structural and functional performance of dissolving MNs. This work contributes to our understanding of how formulation parameters influence the function of MNs, and is aligned with efforts to develop safe, minimally invasive, and efficient transdermal systems that deliver drugs in a controlled and localized way.

Three grades of chitosan (low, medium, and high molecular weight) were selected to investigate how the molecular weight of chitosan affects its mechanical strength, solubility, viscosity, and drug release behavior [18]. In addition, chitosan concentrations of 0.5%, 1.5%, and 3% (w/v) were selected to assess a range of polymer contents. The 0.5% formulation served as a lower structural limit: its very low viscosity was expected to facilitate easy, bubble-free micromold filling and rapid dissolution [19,20]. In contrast, the 3% concentration possessed stronger mechanical properties, though its high viscosity may pose challenges during mold filling and requires more careful fabrication; the resulting dense matrix was anticipated to swell or dissolve slowly, allowing for sustained release [19,21]. The 1.5% concentration was selected to investigate intermediate behavior and potential non-linear trends in performance; this formulation represents an optimal balance between strength, fabricability, and release kinetics.

These formulations were assessed by fabricating nine MN types using the template method, utilizing chitosan with three different molecular weights (LW, MW, and HW) and three concentrations (0.5%, 1.5%, and 3%). PVA/PVP solution was used as the supporting base for the MN matrix. The nine MN types were as follows: 0.5% LW chitosan MNs (0.5LW), 0.5% MW chitosan MNs (0.5MW), 0.5% HW chitosan MNs (0.5HW), 1.5% LW chitosan MNs (1.5LW), 1.5% MW chitosan MNs (1.5MW), 1.5% HW chitosan MNs (1.5HW), 3% LW chitosan MNs (3LW), 3% MW chitosan MNs (3MW), and 3% HW chitosan MNs (3HW). The morphology, mechanical properties, skin insertion, and drug release profiles were characterized and compared using Rhodamine B (RhB) as the model drug. This study provides valuable data on how the molecular weight and concentration of chitosan affect MN performance, which can provide insights into the design of dissolving MNs in transdermal drug delivery.

MATERIALS AND METHODS

Materials

Chitosan of three different weights were purchased from the Vietnam Food Joint Stock Company: LW chitosan (degree of deacetylation $\geq$ 75%, viscosity of 1% solution in 1% acetic acid at 30°C $\leq$ 150.0 cPs); MW chitosan (degree of deacetylation $\geq$ 75%, viscosity of 1% solution in 1% acetic acid at 30°C is around 150–500 cPs); and HW chitosan (degree of deacetylation $\geq$ 75%, viscosity of 1% solution in 1% acetic acid at 30°C $\geq$ 1,000 cPs). These materials were used to prepare chitosan MN patches. Polydimethylsiloxane (PDMS) molds were used to form MN geometries. Each PDMS mold contained a 6 $\times$ 6 array of conical needles (36 MNs/patch) [22]. The dimensions of the mold were as follows: needle height 800 μm, needle base 400 μm, and the tip-to-tip distance of 1200 μm. The chitosan polymer was dissolved in acetic acid (99–100%, Sigma-Aldrich) during sample preparation. RhB (HPLC, $\geq$95%) was obtained from Sigma-Aldrich, 3-(4,5-Dimethyl-2-thiazolyl)-2,5-diphenyl-2H-tetrazolium bromide (MTT reagent) was obtained from St. Louis, MO, USA, and dimethyl sulfoxide (DMSO) was obtained from China.

Nine chitosan solutions were prepared by dissolving three distinct molecular weights (low, medium, and high) and three distinct concentrations (0.5%, 1.5%, and 3%) in acetic acid. PVA/PVP solution was used as the supporting base for the chitosan MNs. Chitosan MNs were fabricated using the double-casting method, with RhB being used as the model drug. Several characteristics of the prepared chitosan MNs were assessed, including morphology, mechanical strength, insertion ability, drug release, and cytotoxicity.

Methods

Preparation of chitosan solution. Predetermined amounts of LW, MW, and HW chitosan were dissolved in 1% v/v of aqueous acetic acid under continuous magnetic stirring for 2 h to obtain chitosan solutions of 0.5% (w/v), 1.5% (w/v), and 3% (w/v). The resulting nine chitosan solutions (0.5% LW, 0.5% MW, 0.5% HW, 1.5% LW, 1.5% MW, 1.5% HW, 3% LW, 3% MW, and 3% HW) were used for chitosan fabrication.

Preparation of PVA/PVP solution. PVA and PVP materials were mixed in a 3:1 ratio to obtain the 20% (w/w) PVA/PVP solution used as the supporting base of the dissolving MNs; this solution has been shown to enhance the mechanical properties of the compound material[23]. Specifically, 1.5 g PVA and 0.5 g PVP (PVA:PVP = 3:1) were dissolved in 10 mL DI water using a magnetic stirrer to obtain a total concentration of 20% (w/w).

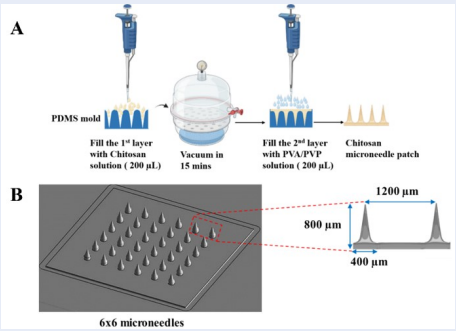

Figure 1: Schematic overview of microneedle fabrication. A) Chitosan MN fabrication process. B) Design of the microneedle patch.

Fabrication of chitosan MNs. The MNs were molded from concentrated chitosan hydrogels using the double-casting method. In contrast to the single-casting approach, double-casting strategically separates the fabrication into two steps: the needle tips are formulated with a drug-loaded polymer optimized for dissolution and delivery, while the backing layer is fabricated from a drug-free polymer blend that possesses superior mechanical strength[24].

First, approximately 200 μL of chitosan hydrogel was spread into a PDMS mold and placed under vacuum for 15 minutes, removing air and ensuring that the chitosan solution completely filled the mold. Subsequently, 200 μL of PVA/PVP solution was loaded into the mold. Finally, the chitosan patches were dried at room temperature for 24 h (Figure 1A). The MN patch was gently removed from the mold using tweezers to obtain the nine different types of chitosan MNs: 0.5LW, 0.5MW, 0.5HW, 1.5LW, 1.5MW, 1.5HW, 3LW, 3MW, and 3HW. The structural design of an MN patch is presented in Figure 1B.

Analysis and characterization of MN morphology. The morphology and integrity of the chitosan MNs were visually examined using the naked eye. The samples were also evaluated using scanning electron microscopy (SEM; JSM-IT100, JEOL). Samples were coated with gold to improve the SEM signal and analyzed at several magnifications to inspect the surface of the nanoparticles. Detailed characteristics of chitosan MN patches evaluated using the ImageJ software, including the width and tip radius of the chitosan MN patches.

Characterization of mechanical properties. The mechanical strength of the chitosan MNs was determined using a force test station equipped with a mechanical sensor[25]. In each test, the chitosan MN was attached to the surface of the platform under a vertically moving mechanical sensor. These sensors compressed the patch to a thickness of 0.8 mm at a rate of 20 mm/h. The travel distance of the sensor and applied force on the MNs were recorded to obtain a force–travel curve for single needles in each array.

Characterization of insertion properties. The insertion capabilities of the MN arrays were investigated using PARAFILM®M, a flexible thermoplastic sheet made of olefin-type material that can be used as a skin simulant for MN insertion tests[26]. In comparison to ex vivo tissue, which often vary due to differences between animal models and require complex preparation, parafilm offers a consistent, rapid, and validated alternative for initial screening[27–29]. Although it does not fully replicate the physiological properties of real skin, studies show that parafilm yields insertion results comparable to those of porcine skin, supporting its use in comparative mechanical performance studies of MN formulations[28,29].

The parafilm sheet was pleated into an eight layers (≈ 1 mm thickness). MN patches were attached to the vertically moving mechanical sensor of the force test station and lowered onto the folded parafilm sheet at a speed of 20 mm/h. The MN arrays were removed after the insertion test and the parafilm sheet unfolded; the number of holes in each layer was counted under a microscope. Insertion was considered successful if more than 20% of holes were formed[26].

Preparation of RhB-loaded chitosan MNs. The modified casting process allows for the encapsulation of model drugs within the MNs. RhB was selected as a fluorescent marker to simulate the release of small,

water-soluble drug molecules from a delivery system. RhB (0.15 wt.%) was mixed with chitosan solution and applied as the first layer of the PDMS mold[26]. Mold cavities were filled using the same process described above. The RhB-loaded chitosan patches were dried at room temperature for 24 h before being gently removed from the mold using tweezers.

***In vitro* drug release from MNs.** To evaluate drug release behavior in vitro, each chitosan MN patch was submerged in 30 mL of 1× PBS (pH 7.4) solution at 37°C. At 5, 15, 30, 60, 120, 240, 480 minutes, and 24 h, 1.0 mL samples were withdrawn and replaced with an equal volume of fresh PBS buffer. The samples were assessed using fluorescence spectrophotometry using a microplate reader with an excitation wavelength and emission wavelength of 553 nm and 627 nm, respectively. The released RhB content was quantified with reference to standard calibration curves.

Cytotoxicity assay. An MTT reduction test was performed to evaluate the viability of mouse fibroblasts (L929 cell line) according to ISO-10993-5-2009[30]. L929 cells were seeded in a 96-well culture disk with 90 μL of medium per well. Samples were tested at concentrations of 0.02, 0.05, 0.09, 0.19, 0.38, 0.75, 1.50, and 3.00 μg/mL. After 24 h of incubation, 10 μL of 3LW was added; untreated wells served as a negative control. The wells continued to be incubated for an additional 24 h. The medium was then removed, and 50 μL of MTT solution was added to each well. After 4 h of incubation, 100 μL of solubilization buffer was added, followed by overnight incubation. Living cells reduce yellow MTT into purple formazan. Since formazan granules are typically insoluble in water, they were dissolved in a buffer solution to allow for quantification. The absorbance of each well was measured at 540 nm to quantify the formazan, which is proportional to the number of viable cells.

Statistical analysis. The data were represented using the mean and standard deviation obtained from at least three independent experiments. Statistical comparisons were performed using one-way analysis of variance (ANOVA) and the Student's t-test in Microsoft Excel 2016. Two-tailed t-tests were performed if there were any statistically significant differences between groups at $p < 0.05$ (*) and $p < 0.001$ (***). NS refers to non-significant results.

RESULTS AND DISCUSSIONS

Morphology of MNs and characteristics analysis

The morphologies of the prepared chitosan MNs were characterized using the naked eye and SEM images.

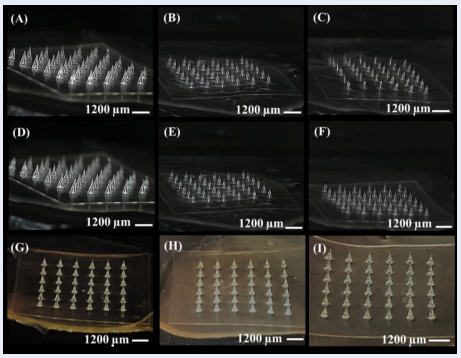

Figure 2: Digital images of chitosan microneedle patches (A) 0.5LW, (B) 0.5MW, (C) 0.5HW, (D) 1.5LW, (E) 1.5MW, (F) 1.5HW, (G) 3LW, (H) 3MW, and (I) 3HW.

Figure 2 shows that all chitosan MN patches exhibited well-defined structures with no missing needles. The chitosan MN patches were arranged in a 6 × 6 array of uniform chitosan MNs, identical to the design of the PDMS mold. No noticeable morphological differences between the nine types of MNs were observed. SEM was used to analyze the structure of the MNs under higher magnifications (Figure 3A1 and Figure 3B1).

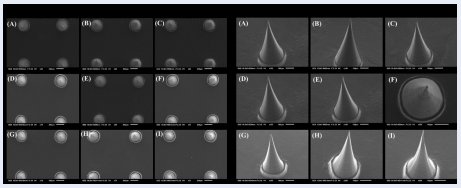

Figure 3: SEM images of chitosan MNs. A1) Plan view of (A) 0.5LW, (B) 0.5MW, (C) 0.5HW, (D) 1.5LW, (E) 1.5MW, (F) 1.5HW, (G) 3LW, (H) 3MW, (I) 3HW. B1) Single-needle images of the same formulations.

The chitosan MNs fabricated from chitosan with different molecular weights exhibited a conical structure with a height of about 730 μm. Figure 4A presents the variation in the base width of each array as a function of their concentrations. The fabricated MNs had a smaller base width (300 μm) than the PDMS master mold (400 μm), indicative of shrinkage in the chitosan arrays. This shrinkage effect increased with both molecular weight and concentration. Among the three types, MNs made from LW chitosan consistently exhibited the largest base width, followed by MW, while HW chitosan produced the smallest base width. At the same concentration, increasing molecular weights reduced the base width. Figure 4B shows

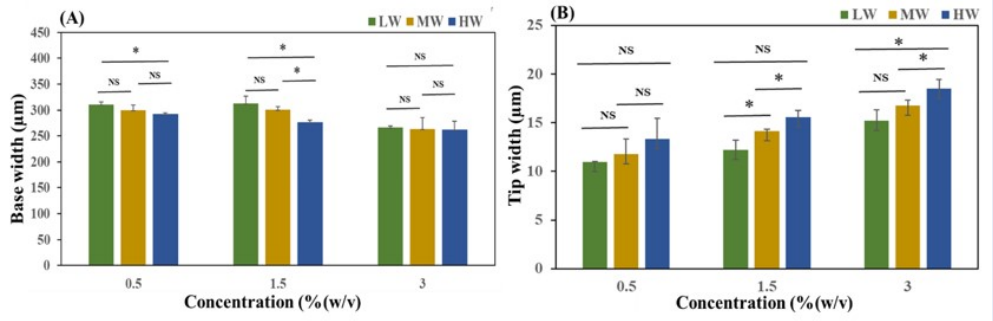

Figure 4: Widths of the chitosan MNs. A) Base width as a function of molecular weight and concentration. B) Tip width under the same conditions. Data are presented as mean ± standard deviation (n = 3). Statistical significance is indicated as $p < 0.05$ (*), while NS indicates non-significant differences.

the tip width of each MN as a function of the molecular weight and concentration. In contrast to the base, the tip width increased with both molecular weight and concentration. This was attributed to the increase in viscosity of the solution, preventing it from filling the cavity during thermal treatment, resulting in wider microneedle tips.

Characterization of mechanical properties

Mechanical strength is a key parameter of MNs, as it determines their ability to reliably and efficiently penetrate skin after topical application. Figure 5 shows the forces at which microneedle failure occurred, allowing for a comparison of the mechanical properties of different chitosan MNs. The minimum force required for a single dissolving MN to penetrate the skin is 0.058 N[31]. Only chitosan MNs prepared at 3% (w/v) concentration (i.e., 3LW, 3MW, and 3HW) exceeded this threshold[32]. The measured forces for 3LW, 3MW, and 3HW were 95.968 mN, 90.473 mN, and 59.105 mN, respectively.

The axial compression test provides a basic assessment of MN strength, with other techniques offering additional insight. Three-point bending tests can evaluate the resistance of the MN to lateral forces as well as help identify fracture points at the baseplate[33]. Repeated-insertion (cyclic loading) tests simulate real-world use by applying multiple penetration cycles to skin simulants, allowing for an assessment of fatigue resistance[34]. These methods provide valuable data on failure modes that are not captured by axial testing alone. Incorporating such evaluations would enable a more comprehensive understanding of MN durability and mechanical reliability.

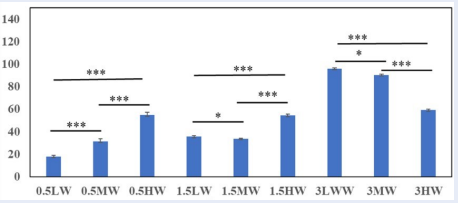

Figure 5: Forces at the point of microneedle failure. Data are presented as mean ± standard deviation (n = 5). Statistical significance is indicated as $p < 0.05$ (*) and $p < 0.001$ (***).

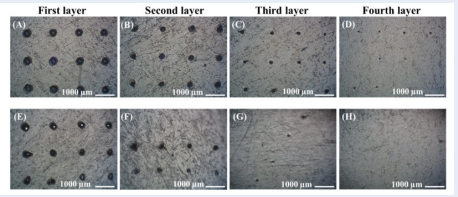

Figure 6: The marks observed in the first, second, third, and fourth parafilm layers after chitosan MNs are removed. (A–D) 3LW, (E–H) 0.5LW.

Characterization of insertion properties

The marks remaining in the first to fourth parafilm layers after the insertion of chitosan MNs are presented in Figure 6 For a successful insertion, at least 20% of needles must penetrate a given parafilm layer. Figure 7 indicates that the successful penetration depth increased with the concentration and molecular weight of chitosan MNs. Specifically, 0.5LW and 0.5MW penetrated the second parafilm layer, 0.5HW penetrated the third parafilm layer, and less than 20% of needles penetrated the fourth parafilm layer. The 1.5LW, 1.5MW, and 1.5HW arrays penetrated the

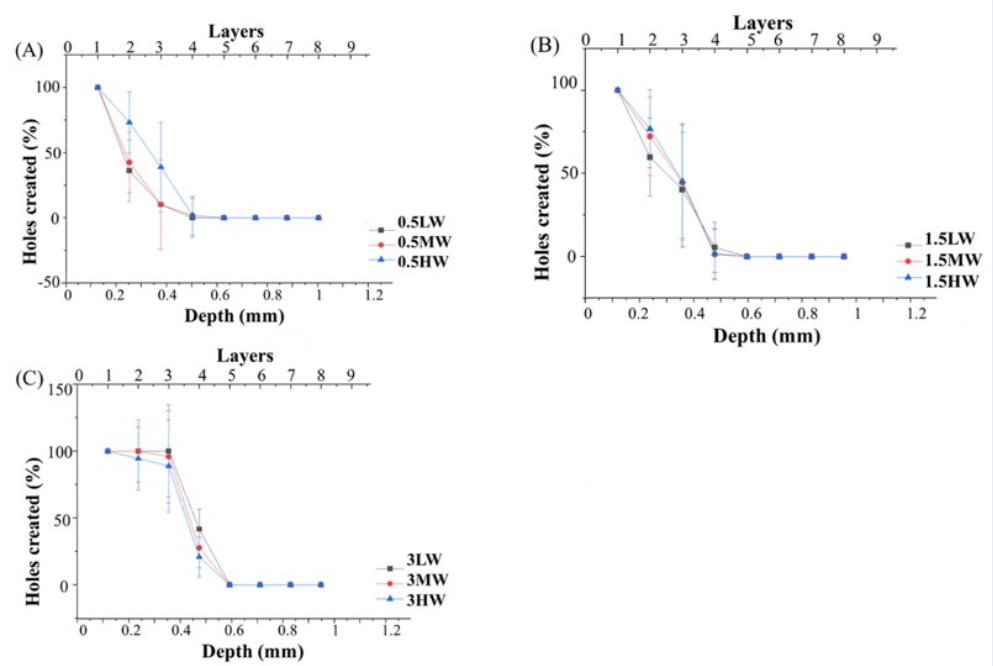

Figure 7: Percentage of holes created in parafilm layers by chitosan MNs as a function of molecular weight for (A) 0.5% (w/v), (B) 1.5% (w/v), and (C) 3% (w/v) chitosan samples.

third layer, with less than 20% penetration into the fourth layer. 3LW, 3MW, and 3HW all penetrated the fourth parafilm layer, with 3LW exhibiting the highest penetration (~41.67%). In general, the 3% chitosan MNs exhibited greater penetration capacity compared to the other chitosan MNs. Since each parafilm layer was 0.13 mm thick, the corresponding insertion depths for each chitosan MN were 0.26 mm for 0.5LW and 0.5MW, 0.39 mm for 0.5HW, 1.5LW, 1.5MW, and 1.5HW, 0.52 mm for 3LW,3MW, and 3HW.

Drug Release from chitosan MNs

The primary selection criteria for the chitosan MNs were mechanical strength and skin insertion capability, as these are essential for effective transdermal delivery[35]. Among all formulations, 3LW exhibited the best performance across both criteria and was consequently selected for further drug release and cytotoxicity testing.

The fluorescence standard curve of RhB in DI water is y = 155.42x with R2 = 0.9962. Figure 8 shows that RhB released from 3LW chitosan microneedle exhibited an initial burst release within 10 min (drug release rate of approximately 61.303%) followed by a slow release over time. The cumulative drug release rate after 24 h was approximately 81.325%.

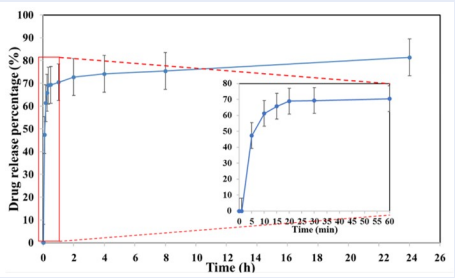

Figure 8: Drug release profile of RhB-loaded 3% LW chitosan MNs.

Cytotoxicity of chitosan solution against the L929 cell line

Since chitosan MNs could potentially be used as wound dressings, biological tests are necessary to ascertain their safety. A material is considered cytotoxic if cell viability after 24 h exposure falls below 70%[30]. Figure 9 shows that the 3LW chitosan solution exhibited a cell viability of 76.005%, indicating that the sample was low-cytotoxic to mouse fibroblasts (L929 cell lines).

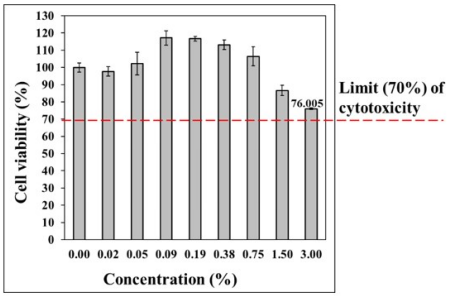

Figure 9: Viability of mouse fibroblasts (L929 cell line) after 24 h exposure to different concentrations of chitosan solution.

CONCLUSIONS

This study aimed to investigate the effect of the molecular weight and concentration of chitosan on the fabrication of MNs for transdermal drug delivery. Using a PVA/PVP solution as the supporting base, nine types of chitosan MNs with varying molecular weights and concentrations were fabricated using the double-casting technique. Using RhB as the model drug, the morphology, mechanical properties, skin insertion properties, cytotoxicity, and drug release profiles of each chitosan MN were evaluated to provide insights into the design of dissolving MNs for transdermal medication delivery.

The morphology, mechanical strength, and insertion properties of the fabricated chitosan MNs were significantly affected by their molecular weight. LW, MW, and HW chitosan MNs at 3%(w/v) concentrations exhibited the greatest mechanical strength. In particular, the 3LW chitosan MN displayed the highest skin penetration using a parafilm skin simulant with an insertion depth $\approx$ 0.52 mm.

Based on these results, the 3LW sample was selected for additional cytotoxicity and drug release profile analyses. Drug release studies revealed an initial burst release within 10 minutes, followed by a slow release over time, highlighting its capability for controlled drug release. Cytotoxicity testing confirmed that 3LW MNs were non-toxic to L929 fibroblasts. These results suggest that chitosan MNs could represent a promising approach for safe and effective transdermal drug delivery.

ABBREVIATION

MNs: microneedles
RhB: rhodamine B
LW: low molecular weight
MW: medium molecular weight
HW: high molecular weight
0.5LW: 0.5% (w/v) low molecular weight chitosan
1.5LW: 1.5% (w/v) low molecular weight chitosan
3LW: 3% (w/v) low molecular weight chitosan
MTT: 3-(4,5-dimethyl-2-thiazolyl)-2,5-diphenyl-2H-tetrazolium bromide
PDMS: polydimethylsiloxane
PVA: polyvinyl alcohol
PVP: polyvinylpyrrolidone

AUTHORS' CONTRIBUTIONS

Bao-Nhien Au: Writing– original draft, Investigation, Formal analysis, Validation, Data curation.
Thuy-Linh Thi Ta: Writing– original draft, Investigation, Formal analysis, Validation, Data curation.
Thanh-Qua Nguyen: Validation, Methodology, Supervision, Conceptualization.
Long Binh Vong: Writing– review & editing, Writing– original draft, Supervision, Resources, Project administration, Investigation, Conceptualization.

COMPETING INTERESTS

The authors have no conflict of interest to declare.

ACKNOWLEDGEMENTS

This work was supported by Vietnam National University Ho Chi Minh City (VNU-HCM) under grant numbers DN2023-28-01.

REFERENCES

1. Ruela AL, Perissinato AG, Lino ME, Mudrik PS, Pereira GR. Evaluation of skin absorption of drugs from topical and transdermal formulations. Braz J Pharm Sci. 2016;52(3):527–44. Available from: https://doi.org/10.1590/S1984-82502016000300018.
2. N'Da DD. Prodrug Strategies for Enhancing the Percutaneous Absorption of Drugs. Molecules. 2014;19(12):20780–20807. Available from: https://doi.org/10.3390/MOLECULES191220780.
3. Prausnitz MR, Langer R. Transdermal drug delivery. Nature Biotechnology. 2008;26(11):1261–1268. Available from: https://doi.org/10.1038/nbt.1504.
4. Gupta M, Agrawal U, Vyas SP. Nanocarrier-based topical drug delivery for the treatment of skin diseases. Expert Opin Drug Deliv. 2012;9(7):783–804. Available from: https://doi.org/10.1517/17425247.2012.686490.
5. Liu T, Chen M, Fu J, Sun Y, Lu C, Quan G, et al. Recent advances in microneedles-mediated transdermal delivery of protein and peptide drugs. Acta Pharm Sin B. 2021;11(8):2326–43. Available from: https://doi.org/10.1016/J.APSB.2021.03.003.
6. Waghule T, Singhvi G, Dubey SK, Pandey MM, Gupta G, Singh M, et al. Microneedles: A smart approach and increasing potential for transdermal drug delivery system. Biomed Pharmacother. 2019;109:1249–58. Available from: https://doi.org/10.1016/J.BIOPHA.2018.10.078.
7. Larrañeta E, Lutton RE, Woolfson AD, Donnelly RF. Microneedle arrays as transdermal and intradermal drug delivery systems: materials science, manufacture and commercial development. Mater Sci Eng Rep. 2016;104:1–32. Available from: https://doi.org/10.1016/J.MSER.2016.03.001.

8. Li S, Li W, Prausnitz M. Individually coated microneedles for co-delivery of multiple compounds with different properties. Drug Deliv Transl Res. 2018;8(5):1043–52. Available from: https://doi.org/10.1007/S13346-018-0549-X.
9. Norman JJ, Choi SO, Tong NT, Aiyar AR, Patel SR, Prausnitz MR, et al. Hollow microneedles for intradermal injection fabricated by sacrificial micromolding and selective electrodeposition. Biomed Microdevices. 2013;15(2):203–10. Available from: https://doi.org/10.1007/S10544-012-9717-9.
10. Rodgers AM, McCrudden MT, Vincente-Perez EM, Dubois AV, Ingram RJ, Larrañeta E, et al. Design and characterisation of a dissolving microneedle patch for intradermal vaccination with heat-inactivated bacteria: A proof of concept study. Int J Pharm. 2018;549(1-2):87–95. Available from: https://doi.org/10.1016/J.IJPHARM.2018.07.049.
11. Chen MC, Ling MH, Lai KY, Pramudityo E. Chitosan microneedle patches for sustained transdermal delivery of macromolecules. Biomacromolecules. 2012;13(12):4022–31. Available from: https://doi.org/10.1021/BM301293D.
12. Bhowmik D, Gopinath H, Kumar BP, Duraivel S, Kumar KPS. THE PHARMA INNOVATION Controlled Release. Drug Deliv Syst. 2012;1(10).
13. Sullivan SP, Murthy N, Prausnitz MR. Minimally invasive protein delivery with rapidly dissolving polymer microneedles. Adv Mater. 2008;20(5):933–8. Available from: https://doi.org/10.1002/ADMA.200701205.
14. Ita K. Dissolving microneedles for transdermal drug delivery: advances and challenges. Biomed Pharmacother. 2017;93:1116–27. Available from: https://doi.org/10.1016/J.BIOPHA.2017.07.019.
15. Ways TMM, Lau WM, Khutoryanskiy VV. Chitosan and Its Derivatives for Application in Mucoadhesive Drug Delivery Systems. Polymers (Basel). 2018;10(3):267. Available from: https://doi.org/10.3390/polym10030267.
16. Chitosan: An Update on Potential Biomedical and Pharmaceutical Applications; 2025.
17. Tian M, Tan H, Li H, You C. Molecular weight dependence of structure and properties of chitosan oligomers. RSC Adv. 2015;5(85):69445–52. Available from: https://doi.org/10.1039/C5RA08358C.
18. Chandrasekharan A, Hwang YJ, Seong KY, Park S, Kim S, Yang SY. Acid-Treated Water-Soluble Chitosan Suitable for Microneedle-Assisted Intracutaneous Drug Delivery. Pharmaceutics. 2019;11(5):209. Available from: https://doi.org/10.3390/pharmaceutics11050209.
19. Bonfante G, Lee H, Bao L, Park J, Takama N, Kim B. Comparison of polymers to enhance mechanical properties of microneedles for bio-medical applications. Micro and Nano Systems Letters. 2020;8(1):13. Available from: https://doi.org/10.1186/s40486-020-00113-0.
20. Badhe RV, Adkine D, Godse A. Development of Polylactic Acid and Bovine Serum Albumin-layered-coated Chitosan Microneedles Using Novel Bees Wax Mould. Turk J Pharm Sci. 2021;18(3):367–75. Available from: https://doi.org/10.4274/tjps.galenos.2020.47897.
21. Thiolated Chitosan Microneedle Patch of Levosulpiride from Fabrication, Characterization to Bioavailability Enhancement Approach; 2025.
22. Pham HP, Le MP, Tran LG, Nguyen TQ. Fabrication and Evaluation of Silk Microneedle Using Replica Molding from Milled Master Mold. IFMBE Proc. 2024;95:573–82. Available from: https://doi.org/10.1007/978-3-031-44630-6_47.
23. Zhuang J, Rao F, Wu D, Huang Y, Xu H, Gao W, et al. Study on the fabrication and characterization of tip-loaded dissolving microneedles for transdermal drug delivery. Eur J Pharm Biopharm. 2020;157:66–73. Available from: https://doi.org/10.1016/J.EJPB.2020.10.002.
24. Qiang N, Liu Z, Lu M, Yang Y, Liao F, Feng Y, et al. Preparation and Properties of Polyvinylpyrrolidone/Sodium Carboxymethyl Cellulose Soluble Microneedles. Materials (Basel). 2023;16(9):3417. Available from: https://doi.org/10.3390/ma16093417.
25. Wang QL, Ren JW, Chen BZ, Jin X, Zhang CY, Guo XD. Effect of humidity on mechanical properties of dissolving microneedles for transdermal drug delivery. J Ind Eng Chem. 2018;59:251–8. Available from: https://doi.org/10.1016/J.JIEC.2017.10.030.
26. Larrañeta E, Moore J, Vicente-Pérez EM, González-Vázquez P, Lutton R, Woolfson AD, et al. A proposed model membrane and test method for microneedle insertion studies. Int J Pharm. 2014;472(1-2):65–73. Available from: https://doi.org/10.1016/J.IJPHARM.2014.05.042.
27. Larrañeta E, Moore J, Vicente-Pérez EM, González-Vázquez P, Lutton R, Woolfson AD, et al. A proposed model membrane and test method for microneedle insertion studies. Int J Pharm. 2014;472(1-2):65–73. Available from: https://doi.org/10.1016/j.ijpharm.2014.05.042.
28. Anjani QK, Nainggolan AD, Li H, Miatmoko A, Larrañeta E, Donnelly RF. Parafilm®M and Strat-M®as skin simulants in in vitro permeation of dissolving microarray patches loaded with proteins. Int J Pharm. 2024;655. Available from: https://doi.org/10.1016/j.ijpharm.2024.124071.
29. Alrimawi BH, Lee JY, Ng KW, Goh CF. In vitro evaluation of microneedle strength: a comparison of test configurations and experimental insights. RSC Pharm. 2024;1(2):227–33. Available from: https://doi.org/10.1039/d4pm00024b.
30. Gao Y, Hou M, Yang R, Zhang L, Xu Z, Kang Y, et al. Highly Porous Silk Fibroin Scaffold Packed in PEGDA/Sucrose Microneedles for Controllable Transdermal Drug Delivery. Biomacromolecules. 2019;20(3):1334–45. Available from: https://doi.org/10.1021/ACS.BIOMAC.8B01715.
31. Biological evaluation of medical devices-Part 5: Tests for in vitro cytotoxicity.
32. Park JH, Allen MG, Prausnitz MR. Biodegradable polymer microneedles: fabrication, mechanics and transdermal drug delivery. J Control Release. 2005;104(1):51–66. Available from: https://doi.org/10.1016/J.JCONREL.2005.02.002.
33. Sirbubalo M, Tucak A, Muhamedagic K, Hindija L, Rahić O, Hadć J, et al. 3D Printing-A -Button"Approach to Manufacture Microneedles for Transdermal Drug Delivery. Pharmaceutics. 2021;13(7):924. Available from: https://doi.org/10.3390/pharmaceutics13070924.
34. Mishra R, Pramanick B, Maiti TK, Bhattacharyya TK. Glassy carbon microneedles-new transdermal drug delivery device derived from a scalable C-MEMS process. Microsyst Nanoeng. 2018;4(1):38. Available from: https://doi.org/10.1038/s41378-018-0039-9.
35. Al-Japairai KAS, Mahmood S, Almurisi SH, Venugopal JR, Hilles AR, Azmana M, et al. Current trends in polymer microneedle for transdermal drug delivery. Int J Pharm. 2020;587. Available from: https://doi.org/10.1016/j.ijpharm.2020.119673.